113: Satellite-Based Analysis of Ecological Controls For Land-Surface Evaporation Resistance

STEVEN W RUNNING AND JOHN S KIMBALL

Q1 • *NTSG University of Montana, Missoula, MT, US*

Lack of available water constrains ecological processes for two-thirds of the earth's biosphere. These water limitations are manifested as either physical water deficiency or as a chemical unavailability of water as a result of being frozen. This article summarizes global principles of water limitations on the biosphere, and physiological limitations on plants. It presents hydrometeorological principles of evapotranspiration and organizing logic of the soil–vegetation–atmosphere transfer models commonly used to compute evapotranspiration. We then introduce remote sensing from both optical/thermal and active/passive microwave sensors for calculating landscape scale evapotranspiration. Finally, we offer a multisensor-based integrated surface resistance to define landscape water availability under all conditions.

GLOBAL EXTENT OF WATER LIMITATIONS ON THE BIOSPHERE

EQ1 Water in an available• physical–chemical state is a fundamental property of the land surface in Earth systems science. Presence of liquid water is a requirement for life, so the activity of the biosphere is intimately related to the ever-changing conditions of water on the landscape. Water availability is the primary limiting factor for vegetation growth over roughly two-thirds of the Earth (Nemani *et al.*, 2003). At the most general, global scale, the role of water in the biosphere has two dimensions. First, is the abundance of water, or most commonly the limitations of seasonally suboptimal water supply on vegetation physiology. A second consideration is the physical state, or seasonal duration of liquid water on the landscape. Vast areas of the high latitudes have an abundance of water, but that water is in a frozen state for much of the year and largely unavailable for most biological activity.

Two other localized water limitations must be acknowledged before proceeding. Water inundation from flooding or poor topographic drainage exerts a different control on ecosystems, producing anaerobic soil conditions that cause many plants literally to drown from lack of root aeration. Also, water with high salt concentrations occasionally found in desert systems can have osmotic potentials too low for plant tolerance, producing a different kind of chemical water limitation. This article will not deal with these conditions that can be locally severe, but are limited in global scope.

The purpose of this article is to develop a more integrated analysis of primary water limitations on biospheric activity. We can define vegetation by its relative abundance (a forest) or absence (a desert), and by its biological activity, the growing season when the ecosystem biogeochemical cycles are active, as contrasted with the dormant season, when water, carbon, and nutrient fluxes are minimal to zero. In like manner, we can define water also by its activity. The severe absence of water, a drought condition, limits ecosystem activity to a near dormant state until rainfall returns. Water in a frozen state is rather equivalent to vegetation in its dormant state, and in fact freezing of water is a primary cause for vegetation to enter dormancy.

So this more comprehensive measure of water availability to the biosphere requires measuring both the presence of water and its physical frozen or liquid state. The history of remote sensing for these land surface properties is concentrated on optical/thermal and passive microwave sensors for defining water abundance, and active–passive microwave

Encyclopedia of Hydrological Sciences. Edited by M. Anderson.

measures for surface freeze–thaw condition. This article will attempt an analysis combining aspects of all these sensors toward a single measure of water mobility on the landscape. We will recommend a multisensor satellite-based algorithm that can provide an integrated global, year-round evaluation of water availability for the biosphere.

Global Biospheric Patterns and Hydrologic Limits

Biogeographers have for decades related global vegetation distribution to broad indices of temperature and water (Walter, 1979). At global scales, the most obvious explanation for the difference in vegetation between deserts and forests was persistence of available water for plant growth. Water availability was most simply described by supply of annual precipitation, but it was quickly apparent that a more refined approach had to include evaporative demand, or a water balance, precipitation minus potential evapotranspiration (PET). Although the logic for use of these water balances as an environmental index is sound, there are many different formulations and temporal domains. PET can be computed in many different ways using radiation, temperature, humidity, wind speed, and other variables for formulations of varying complexity, and computed for time spans from subhourly to annually (Vorosmarty *et al.*, 1998).

Grier and Running (1977) quantified a more explicit functional relationship between climate and vegetation, observing that leaf area indices (LAI) of forests in Northwest America were directly correlated to an annual water balance. LAI is a more useful definition of vegetation than biomass or height because the functional leaf surface area for evapotranspiration, and canopy interception of radiation and precipitation is quantified directly. Nemani and Running (1989) further developed the soil–vegetation–atmosphere systems logic relating soil water holding capacity and vegetation LAI to meteorological water balances. Similar ideas have also been pursued by Stephenson (1990) and •Eagleson (1999). Q6

Woodward (1987) expanded this analysis to global scales, computing a more sophisticated index of vegetation water balance, and using global climate data to predict both biome distributions and LAI. Prentice *et al.* (1992) and Nielson (1995) use similar water balance computations to predict global vegetation distribution patterns, in what are now known as *Dynamic Global Vegetation Models* (DGVMs). Kergoat (1998) introduced remote sensing to calculating global hydrologic equilibriums for predicting LAI, using biweekly NDVI data to follow the vegetation growing season, or phenology. Most recently, Nemani *et al.* (2003) evaluated climatic controls on global vegetation productivity, and determined that over 40% of the Earth's vegetated surface is limited by low water availability, while approximately 33% is limited by cold temperatures and water in it's frozen state, also limiting water availability for plant growth (Figure 1).

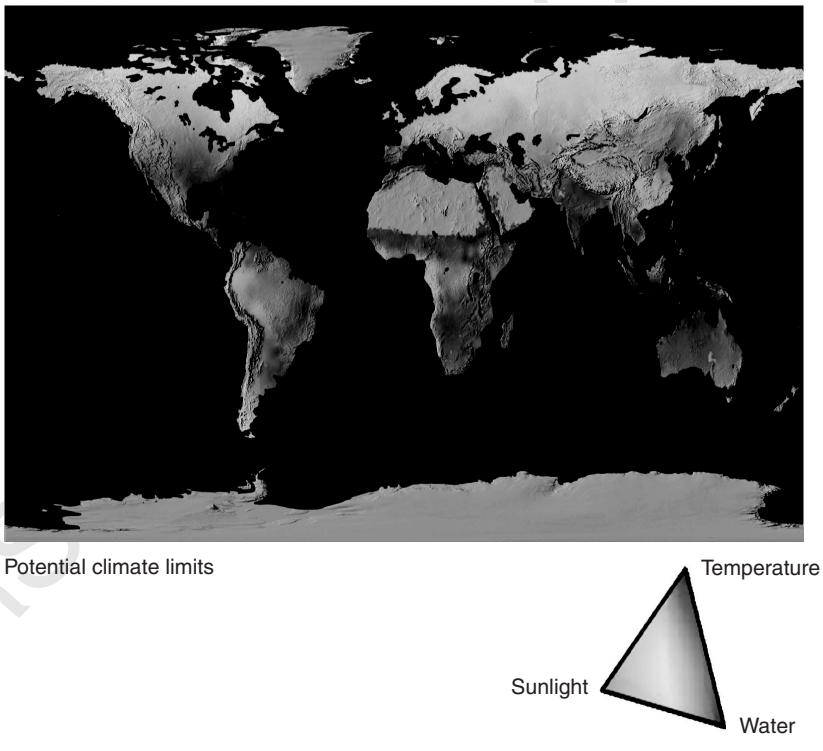

Figure 1 Global analysis of the relative balance of climatic controls on evapotranspiration of vegetation

All of these studies relate water limitations to vegetation structural development over relatively long time scales (i.e. decades). We next evaluate how water controls vegetation biophysics and physiology over more immediate daily to seasonal time domains.

Ecological Principles of Water Limits on Plants

Vegetation responds to water deficits in many ways (Waring and Running, 1998). Even mild soil water deficits begin to inhibit cellular expansion, xylem water flow from roots to leaves and phloem sugar transfer in stems of growing plants. Plant water deficits induce progressive leaf stomatal closure, which reduces plant water loss while bringing photosynthesis, transpiration, and canopy-atmosphere gas exchange nearly to a halt. Sustained drought will produce early leaf senescence and shedding, and may impact ecosystem leaf area for a number of years. Additionally, dry soils reduce soil litter decomposition rates, and related nutrient mobilization. Subzero temperatures and frozen water induce the same ecosystem responses, although the biological mechanics are somewhat different; plant cellular growth is inhibited; stomata are closed, limiting photosynthesis, gas exchange, and transpiration; water movement across root membranes, xylem sap flow, soil decomposition, and plant nutrient uptake are severely restricted. When plants are in a fully frost tolerant state, water molecules are hydroscopically bound to cell walls, minimizing ice crystal formation and cellular rupture. It is the lack of these cold tolerant mechanisms that restricts tropical plants to climates that never experience freezing temperatures. Consequently, lack of mobile water, either from the absence of liquid water or from freezing, has similar impacts on reducing plant leaf area, transpiration, growth, and related ecosystem activity.

Hydrometeorological Principles of Vegetation Limits on Evapotranspiration

For meteorological processes, land surface water status and frozen or thawed state determine whether the incident radiant energy is dissipated by heating the air and soil, or by evaporating or sublimating water. From energy balance theory it is clear that:

$$R_n = H + LE + G \tag{1}$$

Net radiation, R_n, being absorbed by the land surface is predominantly partitioned into H, sensible heat, or LE, latent energy evaporating water ($W\,m^{-2}$), while energy loss through soil conductance and photosynthesis, G, are relatively minor components of the energy budget (<5%) over vegetation so are often ignored. Thus, the summary Bowen ratio:

$$B = \frac{H}{LE} \tag{2}$$

can quantify the wide range of energy partitions found from completely dry surfaces where B approaches infinity, that is, all net radiation is translated into heat, to $B = 0$, an open water surface where nearly all net radiation is used to evaporate water. Quantifying the available water at the land surface and the resistance to surface evaporation from soil and vegetation is key to computing LE.

For hydrologic processes, evaporation is quantified as a component of the land surface water budget,

$$PPT = ET + Q + \Delta S \tag{3}$$

where PPT, ET, Q, and ΔS represent precipitation, evapotranspiration, outflow, and a change in water storage ($kg\,m^{-2}$) per unit time, respectively. The storage term, ΔS, includes both surface and subsurface water storage, including water in the subsurface soil profile that ultimately drains to streamflow or groundwater recharge.

For ecological processes, soil moisture is important for determining litter decomposition rates and soil CO_2 evolution, and for providing available liquid water to plants for transpiration demands. Ultimately, therefore, the availability of water for land surface evaporation is a fundamental constraint and integrator of meteorological, hydrological, and ecological processes.

The most widely accepted formula for computing land surface evaporation is the Penman–Monteith (P–M) equation, which combines the key meteorological drivers for evaporation, net radiation, humidity, and windspeed, with the key surface attributes that control evaporation rates. The surface attributes are defined as resistances, one biologically mediated by leaf area and leaf stomatal dynamics, the other physically related quantifying canopy roughness and aerodynamic exchanges. The P–M equation computes latent energy, or λE

$$\lambda E = \frac{\Delta \cdot r_e \cdot (R_n - G_0) + \rho C_p \cdot (e_{sat} - e)}{r_e \cdot (\gamma + \Delta) + \gamma \cdot r_i} \tag{4}$$

where e and e_{sat} are actual and saturation vapor pressure respectively; γ is the psychrometric constant, and Δ is the rate of change of saturation vapor pressure with temperature (i.e. $\partial e_{sat}(T)/\partial T$); r_i is the bulk surface internal resistance and r_e is the external or aerodynamic resistance. In the above equation, it is assumed that the turbulent exchange characteristics for heat and vapor transfer are the same. The Penman–Monteith equation is strictly valid only for a closed vegetation canopy; however, the formula can be adapted for spars vegetation or even a bare soil surface with properly defined bulk internal diffusion and turbulent transfer resistances.

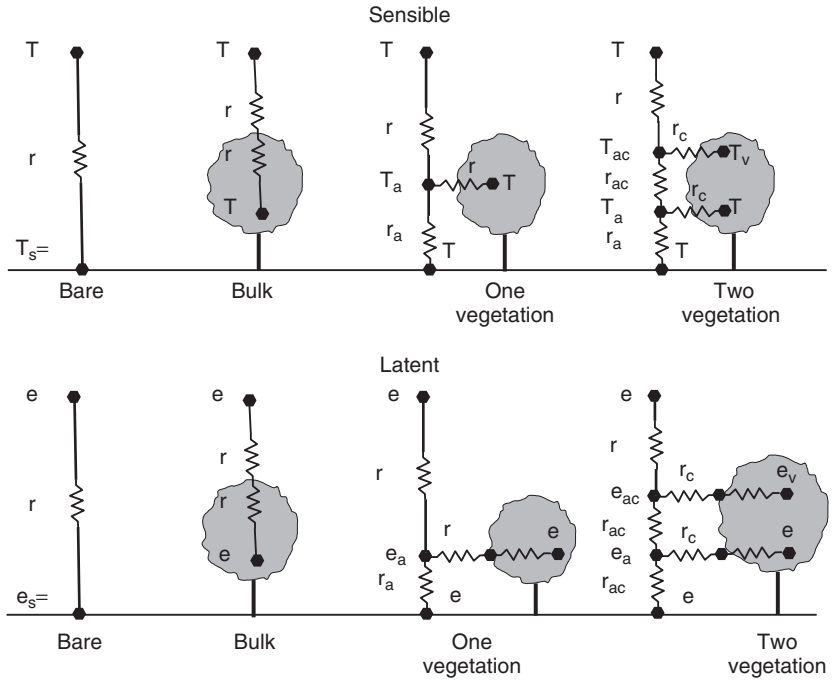

Q2 **Figure 2** Electrical analog theory used• to depict components of meteorology and resistance in transfer of sensible and latent heat from vegetation to the atmosphere. ($T_{a,s,v,g}$ = temperature of air, soil, vegetation, ground; $e_{a,v,g}$ = vapor pressure at atmosphere, vegetation, ground; $r_{a,c,s}$ = resistances at aerodynamic, canopy, surface) From Bonan (2002)

Systems Analysis of Soil–Vegetation–Atmosphere Transfer

Critical to computing accurate surface-atmosphere energy transfer and evaporation rates is the representation of various constraints in the soil–vegetation–atmosphere system. These constraints have classically been defined as resistances using electrical analogue theory (Figure 2). Surface resistance includes a variety of surface properties that impede the evaporation of water from the surface, and can incorporate both physical and biological impediments. For example, vegetation height exerts an aerodynamic roughness that decreases resistance, soil litter exerts a bulk diffusion resistance and vegetation physiological stomatal control increases surface resistance as stomata close in reaction to water deficits. Although the P–M equations were derived from electrical analogue theory incorporating resistances, we can simply transform these resistances to their reciprocal, surface conductance, with the advantage that surface conductances are then directly, rather than inversely proportional to the final evaporation rates.

Beginning in the 1970s these concepts were organized into a variety of SVAT (Soil–Vegetation–Atmosphere Transfer) models (Waring and Running, 1998). Some of these SVAT models were incorporated within atmospheric General Circulation Models, GCMs, like the BATS Biosphere Atmosphere Transfer Scheme of Dickinson (1996) and SiB Simple Biosphere model (Sellers *et al.*, 1986). The Project for Intercomparison of Land Surface Models analyzed the various logics and structures for these models (Pitman, 2003). Other SVAT models were designed to work in ecological biogeochemistry modeling such as FOREST-BGC (Running and Coughlan, 1988) or in hydroecological modeling (Band *et al.*, 1993).

A simple SVAT model flowchart is shown in Figure 3 (Bonan, 2002). Critical hydrologic components include precipitation, snowpack, and soil water storage, surface, and subsurface runoff. These topics are covered in detail elsewhere and in other articles. For this article, we now focus on evaporation and transpiration processes, and the control of these rates by the surface resistance. The total, or bulk surface resistance, integrates aerodynamic, soil, and canopy resistances to evaporation, and the physiological control of stomatal dynamics to vegetation transpiration. These resistance components are often dealt with separately, but landscape evapotranspiration rates are constrained by this total surface resistance.

REMOTE SENSING PRINCIPLES FOR EVAPOTRANSPIRATION

Remote sensing provides a particularly valuable methodology for evaluating total surface resistance, because the satellite sensor inherently views the entire land surface, not separating vegetation from soil. The reflectance, emission, or backscatter of electromagnetic energy as observed from a

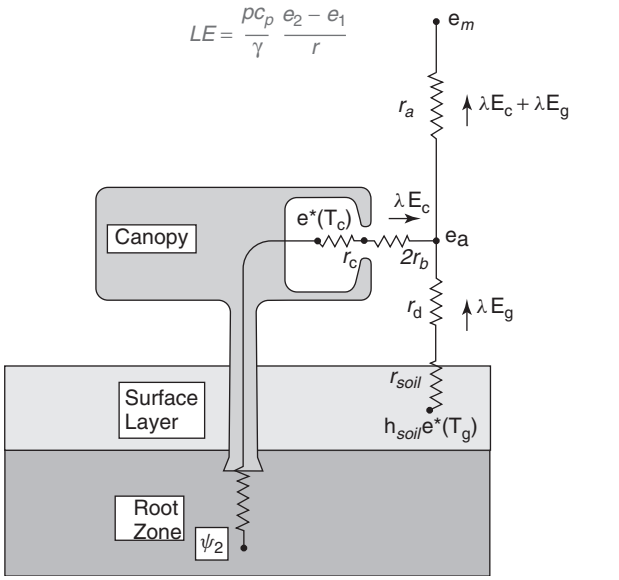

Q7 **Figure 3** Diagram of a simple SVAT• or Soil–Vegetation–Atmosphere Transfer model. ($\lambda E_{c,g}$ = latent energy from canopy, ground; $r_{a,c,b}$ = resistance from aerodynamic, canopy, boundary layer. Other symbols in text.) From Bonan (2002)

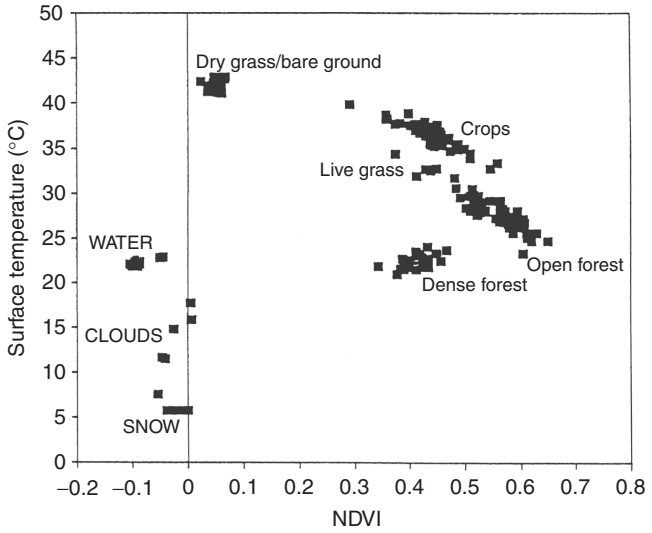

Figure 4 Ranges of radiometric• surface temperature LST, and NDVI observed for a 106 000 km^2 landscape of western Montana on 14 July 1987 from AVHRR. Water clouds and snow all have low NDVI and very cool radiometric temperatures compared to the vegetated landscape, with dry bare ground the warmest. From Nemani and Running (1989) Q8

satellite sensor provides an integrated view of the landscape dependant on the spatial resolution of the dataset. With any sensor of spatial resolution larger than approximately 5 m, individual plants are not resolved, and a combined view of multiple plants and the surrounding soil or litter surfaces are always included. Rather than attempting to laboriously separate vegetation from soil, or limiting analysis only to completely vegetated or bare soil surfaces, satellite remote sensing lends itself well to evaluating the total landscape resistance to surface-atmosphere energy and mass exchange.

The evaporation theory summarized above is very well developed, and measurement of land surface evaporation and conductance constraints is rather routine for plot scales. The challenge now is to represent regional and continental scales with this theory. The meteorological drivers in the P–M equation are regularly available from mesoscale to global-gridded meteorological models. Representing the extreme spatial and temporal heterogeneity of surface resistances is the biggest limitation for accurate measures of evaporation at landscape to continental scales. At these scales, remote sensing data are readily available, and consequently a variety of sensors have been explored for both direct and indirect assessment of evaporation and associated surface resistances to water and energy movement.

Optical/Thermal Sensors

Optical and thermal sensors provide two key attributes for quantifying land surface evaporation. First, these sensors are sensitive to photosynthetic biomass and surface temperature, and are useful for quantifying vegetation cover and canopy leaf area index. Structural, phenological, and other morphological differences among major vegetation types (e.g. forests, grasslands, croplands) are defined by land cover classes distinguished using optical/thermal sensors like MODIS (Figure 4). Evaluating seasonal trajectories of vegetation indices such as NDVI and land surface temperature (LST) provides an additional dimension of biome discrimination, as more open and arid vegetation types show dramatically higher LST (Figure 5). Global 1 km resolution datasets of general land cover classes that include simple vegetation biome discrimination are now regularly available and are updated annually to reflect land cover changes (Friedl *et al.*, 2002). Higher resolution land cover data are also available based on 30-m resolution Landsat data, allowing more precise vegetation cover discrimination (•Vogelmann *et al.*, 2002). Newer generation land cover mapping methods avoid logical classification errors by computing continuous fields of fractional vegetation cover that are then directly interpretable for defining surface roughness, albedo, and LAI for evaporation calculations (Hansen *et al.*, 2002). Q9

NIR/red spectral band ratios such as the NDVI are widely used to estimate vegetation LAI over large areas (Myneni *et al.*, 2002). Increasing LAI provides greater cumulative surface area for canopy water interception and evaporation, and for transpiration by vegetation canopies. Higher LAI also infers more robust vegetation with deeper

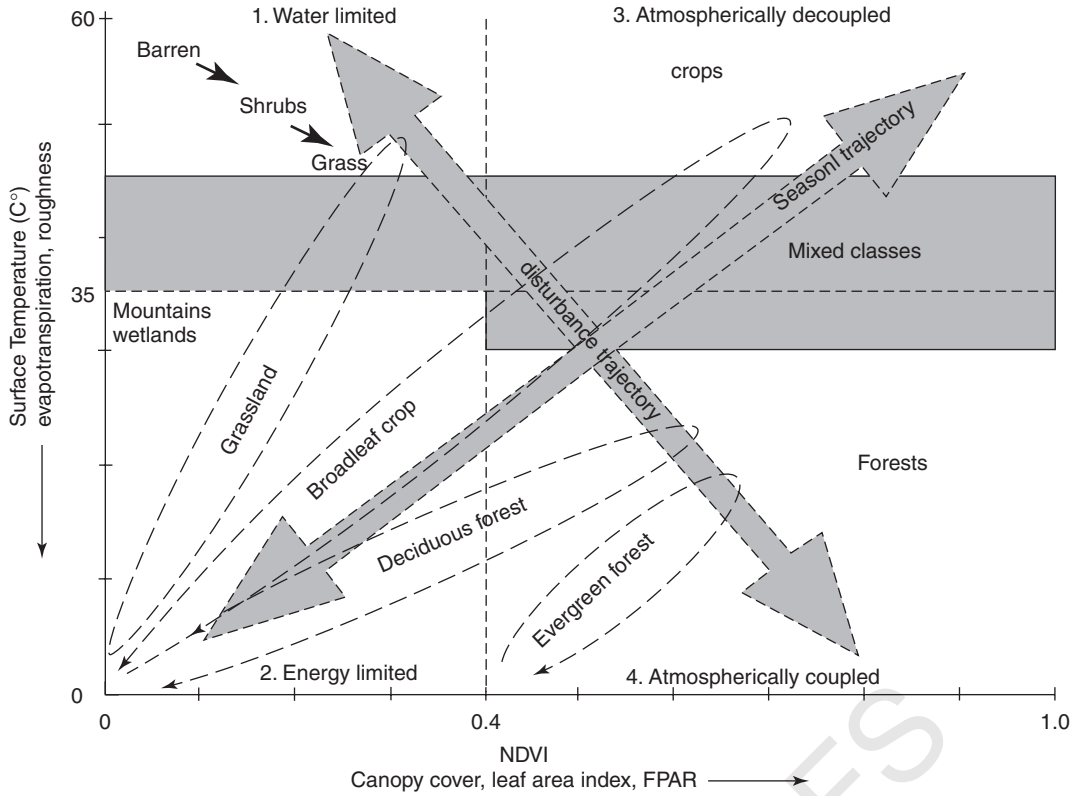

Q3 **Figure 5** Separation of biome• types possible by following the seasonal time series of radiometric surface temperature LST and NDVI. As vegetation grows in the spring NDVI and LST rise, but at different rates depending on the surface energy exchange characteristics of the vegetation. As vegetation desiccates in late summer, or with disturbances, NDVI falls and LST rises. From Nemani and Running (1997)

rooting zones that are able to tap water deeper in the soil profile, thus allowing an indirect measure of deeper soil water availability than surface observations alone can directly provide.

Thermal remote sensing of radiometric land surface temperature, LST, most directly measures the sensible heat component of the energy balance, and is thus inversely proportional to latent energy and evaporation rates (Wan *et al.*, 2002). As previously discussed, the Bowen ratio (H/LE) is a relatively simple parameter summarizing the relationship between sensible and latent heat flux from a surface. Land surfaces can vary from a very high Bowen ratio when completely dry, often more than 10, to as low as 0.1 when wet. These changes in land surface energy partitioning can occur slowly as a vegetated landscape dries out over many weeks during summer, and then abruptly as the Bowen ratio drops following a substantial rainfall event. Thermal remote sensing can provide an integrated look at land surface evaporation, although overpass timing is critical, as midafternoon radiant heating of the land surface provides the most useful signal. Historically, the NOAA AVHRR sensor with 1430 local overpass time has been most valuable, and now the MODIS sensor on the 1330 Aqua platform is providing high-quality LST data. For some purposes, geostationary satellite data from GOES also can be used to derive LST and surface ET every hour under cloud-free conditions (Norman *et al.*, 2003; Diak *et al.*, 2004).

Many studies have combined both spectral vegetation index and LST information from satellite optical/infrared sensors to infer land surface evaporation rates, typically as a ratio of LST/NDVI (Gillies *et al.*, 1997; Sandholt *et al.*, 2002; Moran *et al.*, 1994; Goward *et al.*, 2002). The denominator, NDVI or equivalent, quantifies potential *increases* in evaporation due to more evaporating surface of LAI, while the numerator, LST infers *decreases* in evaporative conductance from increases in sensible heat. If we examine a single scene of a complex natural landscape in midsummer, a logical pattern of NDVI and LST is discernible (Figure 5, Nemani and Running, 1989). In this Montana mountainous landscape, clouds and snow are shown with low NDVI and low LST, mesic forests have a high NDVI but rather cool LST, and dry grasses or bare land show low NDVI but high LST. This surface discrimination is strongest during midsummer conditions under relatively high surface solar energy loading with spatially

heterogeneous energy partitioning and associated LSTs. As a surface dries, the LST pattern becomes progressively higher and can easily exceed 60 °C, even with screen-height air temperatures below 40 °C (Figure 6a). By quantifying temporal changes in the slope of the maximum LST/NDVI curve, an inference of surface resistance can be made (Figure 6b; Nemani *et al.*, 1993; Nishida *et al.*, 2003).

However, when we attempt to monitor a region regularly through the vegetation growing season, the most fundamental constraint is the regular interruption by cloudiness and atmospheric aerosols that limit clear imaging of the land surface. In humid tropical areas, cloud cover limits optical/infrared remote sensing more than 80% of the year, and latitudes above 50 degrees also have extended periods of summer cloudiness (Figure 7). For these situations of extended cloudiness and/or inadequate seasonal solar illumination, microwave sensors provide the potential

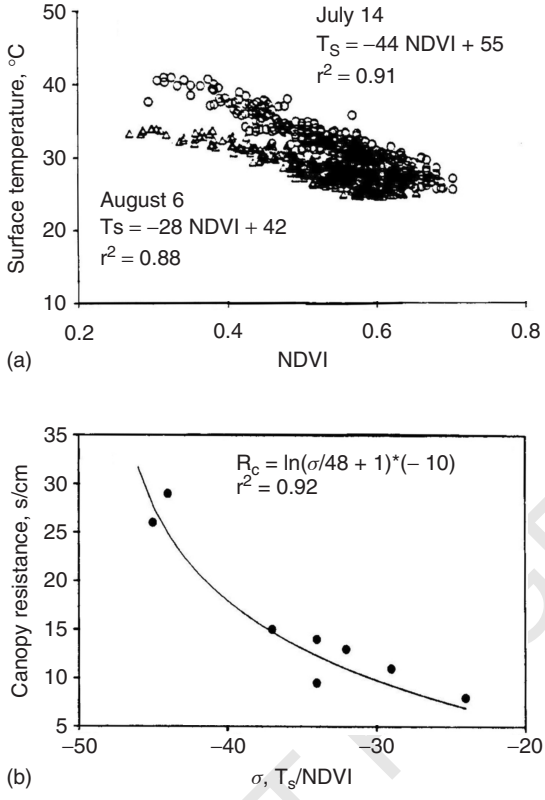

Q10 **Figure 6** (a) Change in the slope• of the LST/NDVI relationship from 14 July, after extended drought, and 6 August, after 3.2 cm of rain, for a natural landscape in western Montana, as observed by AVHRR. A reduction in Bowen ratio is evident in the reduced LST after substantial rainfall. (b) A canopy resistance, simulated by the SVAT model, FOREST-BGC, was highly correlated with seasonal changes in slope of the LST/NDVI relationship, suggesting a way to infer surface resistances by satellite over large regions. From Nemani and Running (1989), Nemani *et al.* (1993)

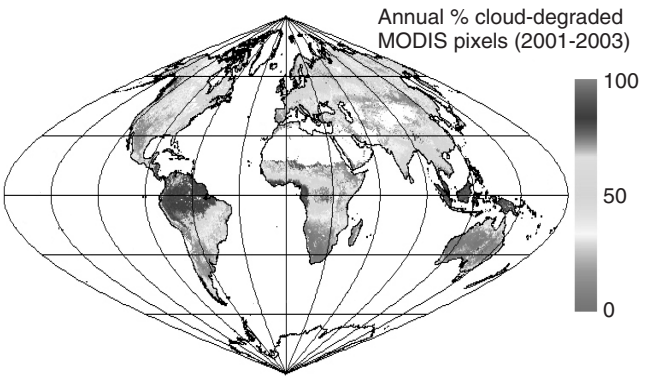

Figure 7 The fraction of annual• MODIS land surface optical reflectance data degraded by cloud cover for 2003. From •Zhao *et al.* (2004) Q11 Q12

for all-weather imaging of the land surface. Remote sensing at microwave wavelengths is largely independent of solar illumination, cloud cover, and other atmospheric attenuation impacts that can significantly degrade remote sensing capabilities at optical and infrared wavelengths. However, microwave wavelengths also provide different information than optical/infrared wavelengths and must be evaluated in a different way.

Active/Passive Microwave Sensors

Microwave remote sensing occurs over much longer spectral wavelengths (0.1 to 30 cm) than optical/NIR remote sensing (0.4 to 10 μm). The signal detected by an active or passive microwave sensor is a function of the emission, absorption, transmission, scattering, and reflectivity of electromagnetic (EM) energy by the landscape and intervening atmosphere at a given spectral wavelength (Ulaby *et al.*, 1986). These properties, in turn, are sensitive to changes in the physical characteristics of the landscape including, surface structure, roughness, orientation, and dielectric properties. At the microwave wavelengths most commonly used for Earth remote sensing, the atmosphere is largely transparent with minimal attenuation of EM energy.

The dielectric constant characterizes the electrical properties and propagation of EM energy in the landscape (El-Rayes and Ulaby, 1987). The interaction of EM energy with a dielectric material has its origin in the response of charged particles to the applied field. The displacement of these particles from their equilibrium positions gives rise to induced dipoles that respond to the applied field. In addition, polar materials contain permanent dipoles caused by the asymmetric charge distribution within the molecules themselves. Water is relatively unique in that it has strong molecular (positive, H^{+2}, and negative, O^{-2}) polarity, exhibiting a dielectric constant that dominates the microwave response of natural landscapes (Kraszewski, 1996). Water molecules

in a liquid state align themselves with an applied EM field, while water molecules in ice are bound in a crystalline lattice and cannot freely rotate, resulting in a substantially lower dielectric constant.

Most natural materials have a dielectric constant ranging from 3 to 8 when dry, while liquid water has a dielectric constant of approximately 80 (Ulaby *et al.*, 1986). Thus, short-term variability in landscape radar backscatter and microwave emissions is to a large extent, a function of changes in the moisture status of vegetation, surface, and soil media. Variations in the predominant frozen or thawed state of the landscape also have a major impact on microwave emissions and reflectivity because frozen water has a very low dielectric constant of approximately 2, which is similar to very dry soil.

In seasonally frozen environments, the most dynamic temporal changes in microwave emissions and reflectivity occur in response to seasonal freeze–thaw transitions

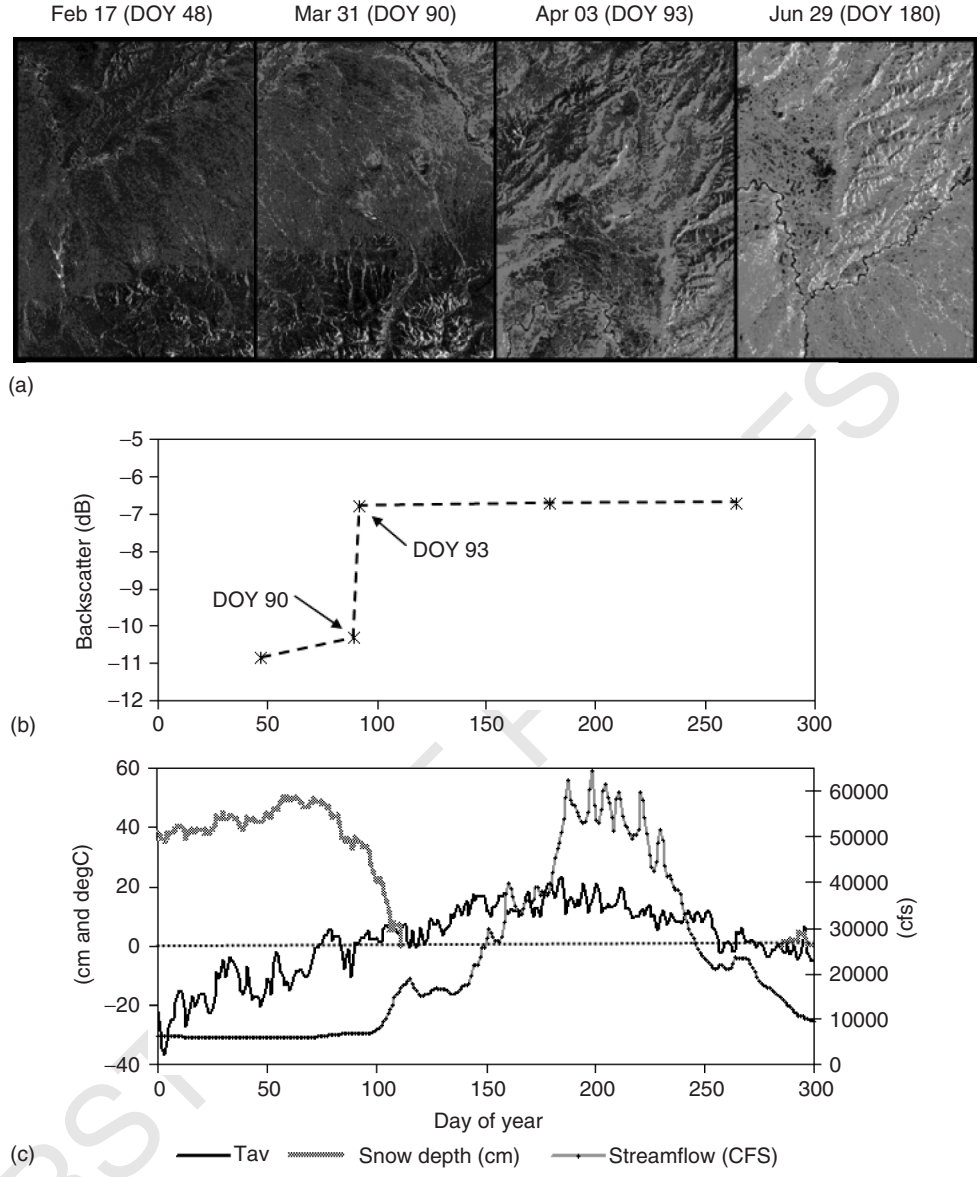

Figure 8 (a)Temporal series of JERS-1 SAR images acquired over interior Alaska boreal forest. The image series shows the landscape radar backscatter transition from predominantly frozen to thawed conditions during spring, 1998. The middle plot (b) shows the radar backscatter temporal response averaged over four sites within the domain. Q4 •(c) Freeze–thaw transitions dominate the 3–5 dB seasonal variation in radar backscatter. A pronounced backscatter increase between days (DOY) 90 and 93 coincides with thawing air temperatures (T_{av}), seasonal snowmelt and the new release of water on the landscape indicated by local weather station data and USGS streamflow records (redrawn from Entekhabi *et al.*, 2004)

(Way *et al.*, 1997; Zhang *et al.*, 2003). Spring thaw and the disappearance of seasonal snow cover in these environments is often rapid due to moderate air temperatures and increasing solar radiation, resulting in large decreases in surface albedo of up to 80% between snow covered and snow free conditions (Zhang *et al.*, 2003). The images in Figure 8 show a temporal sequence of JERS-1 satellite L-Band Synthetic Aperture Radar (SAR) images that capture a seasonal freeze–thaw transition event in the boreal forest region of Alaska (Entekhabi *et al.*, 2004). The pronounced increase in radar backscatter between days 90 and 93 occurs in response to seasonal thawing, snowmelt, and the new release of water on the landscape as indicated by seasonal increases in regional stream flow. This event and other freeze–thaw transitions dominate the 5–6 dB seasonal variation in radar backscatter. The surface resistance to evaporation under frozen conditions is similar in magnitude to that of arid, desert environments, while resistance is minimal following snowmelt, with evaporation approaching potential rates. These changes are most dramatic at high latitudes where seasonal increases in surface energy and liquid water available for evaporation have important consequences for regional weather patterns, hydrological, and biospheric processes (Bonan *et al.*, 1995; Chapin *et al.*, 2000; Kimball *et al.*, 2001, 2004).

Active and passive microwave remote sensing techniques have proven sensitive to vegetation phenology, water stress, and other changes in vegetation structure and water content, snow cover, and soil moisture (Waring *et al.*, 1995; Kane *et al.*, 1996; Kimball *et al.*, 2004). The ability of microwave remote sensing to detect changes in the moisture status of these various landscape components is strongly dependent on sensor wavelength, polarization, and spatial resolution. Landscape topography, vegetation structure, soil type, the presence/absence and structure of snow cover also influence retrieval accuracies. Longer wavelengths (e.g. L-band) are generally sensitive to a greater volume of surface vegetation and soil media, relative to shorter (Ku-, C-bands) wavelengths under similar conditions. Longer microwave wavelengths are also directly related to soil moisture as long as the overlying vegetation water content is low (i.e. $< 5–6\,\mathrm{kg\,m^{-2}}$). Soil moisture sensitivity is also generally limited to the top 5–10 cm of the surface soil layer even in bare soil environments. At biomass levels roughly above that of a fully developed corn crop, however, the ability of microwave remote sensing to detect soil moisture decreases, while sensitivity to vegetation increases.

Vegetation cover is a major impediment limiting direct microwave remote sensing detection of soil moisture over much of the globe. The relatively coarse spatial scales, band widths, and orbital geometries of all current and planned satellite microwave remote sensing platforms also limit capabilities for resolving subgrid scale differences in the moisture content of individual landscape components. However, these scales are generally optimal for regional assessment and monitoring of bulk, landscape surface resistances to evaporation and a fundamental limitation to latent energy and water exchange with the atmosphere.

INTEGRATED REMOTE SENSING OF LANDSCAPE WATER MOBILITY

Regional to Global Scaling

The regional patterns and temporal dynamics of water mobility and surface resistances of the landscape have important consequences for troposphere boundary layer development, weather and global climate. For example, the seasonal transition between frozen (high surface resistance) and nonfrozen (low surface resistance) conditions in the spring is relatively abrupt and coincident with seasonal snowmelt and runoff, large decreases in surface albedo and the initiation of the growing season at high latitudes and upper elevations. The timing and spatial extent of this seasonal shift is of critical importance to the establishment and location of the polar front and regional to global scale weather patterns (Bonan *et al.*, 1995; Chapin *et al.*, 2000). The timing of this frozen/thawed transition is also a major control on vegetation productivity and regional source-sink strength for atmospheric CO_2 (Kimball *et al.*, 2004; McDonald *et al.*, 2004).

At continental scales, satellite-based approaches have been developed to monitor changes in plant available

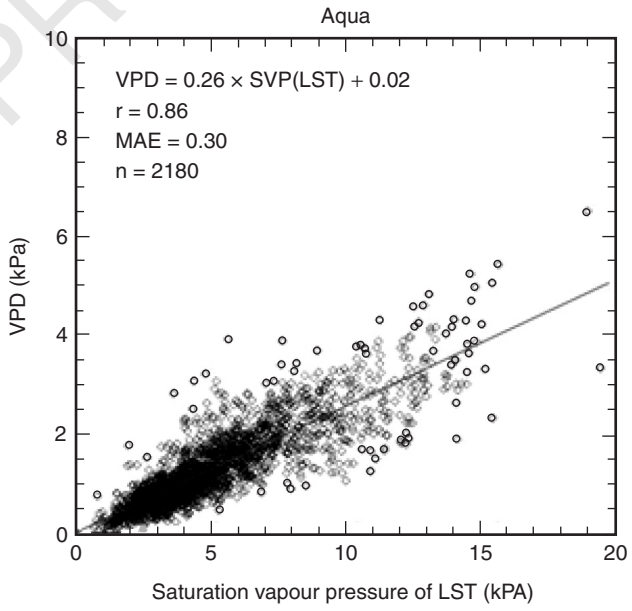

Figure 9 Relationship between a composited maximum 8-day LST from MODIS Aqua at 1330 overpass time and global land surface VPD measured at 2180 surface weather stations for August 2003. From Hashimoto *et al.* (2004) Q13

moisture on the landscape (Nemani *et al.*, 1993; Nishida *et al.*, 2003, Hashimoto *et al.*, 2004). These advancements offer the potential for finer temporal sampling and mitigation of atmospheric interference. For example, improved MODIS radiometric calibration and cloud-screening algorithms allow the assessment of daily LST temporal dynamics for individual sensor footprints. The scatterplot in Figure 9 shows the relationship between Aqua MODIS LST and the surface energy available for evaporation, which is the primary driver of land-atmosphere latent energy and water fluxes. An 8-day time composite of the MODIS Aqua maximum LST for the period provides a metric of changing land surface evaporation resistance that can be mapped at 1 km resolution over regional, continental, and global extents (Figure 10). These technological advances offer potentially simpler techniques for monitoring surface resistances to water mobility compared to earlier methods developed from NOAA AVHRR data using the LST/NDVI ratio technique (e.g. Nemani *et al.*, 1993).

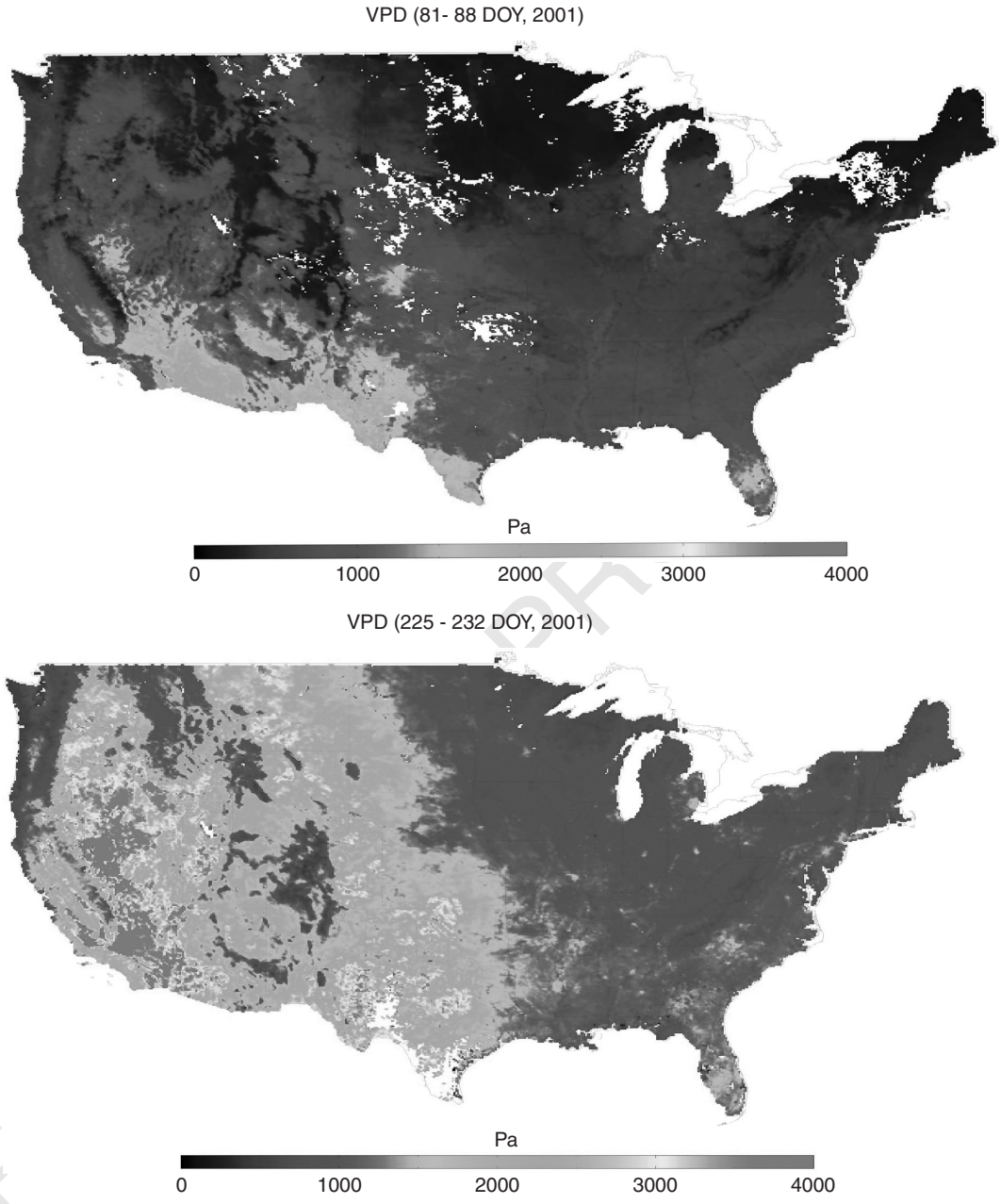

Q5 **Figure 10** Mapping of maximum• weekly VPD during spring and midsummer at 1 km across the continental United States using MODIS Aqua and the relationship in Figure 9. From Hashimoto *et al.* (2004)

Global satellite remote sensing of landscape water mobility at continental scales requires relatively high (e.g. daily) temporal repeat and moderate spatial scales consistent with the development and dynamic nature of regional weather patterns (Schmugge *et al.*, 2002). Evolving weather systems are influenced by land surface characteristics through surface coupling of energy and water fluxes to the atmospheric boundary layer (ABL). The ABL integrates and responds to surface fluxes on the order of 10 km or less (Albertson and Parlange, 2000). The major limitation on the use of satellite optical/infrared methods to monitor landscape water mobility lie primarily with the coarse temporal compositing required to mitigate the effects of clouds, smoke, and other atmospheric aerosols.

The maps in Figure 11 show seasonal extremes of global plant soil water availability for representative early spring and midsummer conditions estimated using an ecosystem process model (Biome-BGC) driven by daily meteorological inputs from an Atmospheric GCM. Areas of low and high soil water availability represent respective surrogates for high and low resistances to surface latent energy, water, and gas exchange with the atmosphere. In winter and early spring, high latitude and upper elevation landscapes are predominantly frozen and have both low water mobility and high resistance to surface-atmosphere exchanges that are of the same order of magnitude as arid desert regions. Areas of low water mobility (high surface resistances) such as arid deserts and frozen regions are dominated by sensible

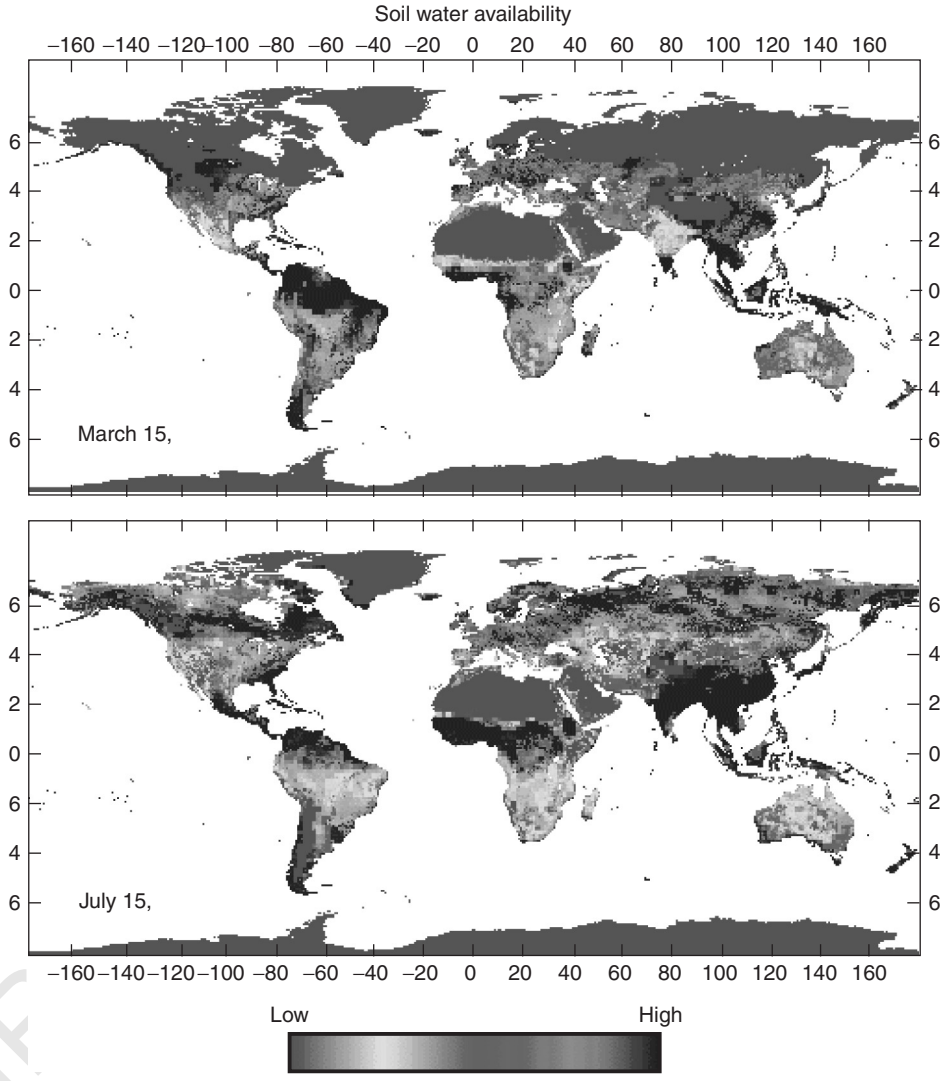

Figure 11 Simulation of a relative integrated soil water availability using NCEP reanalysis daily surface meteorology and the SVAT model Biome-BGC model for 1999. In late winter, 15 March, surface resistance for ET is very high in high latitudes because of freezing temperatures, and in dry deserts. In midsummer, surface resistance is not temperature limited, so high surface resistances are primarily a result of soil water deficits

energy exchange, surface temperature extremes and relatively stable atmospheric conditions. In contrast, areas of high water mobility (low surface resistance) are dominated by latent energy exchange and moderate surface air temperatures. Boreal and arctic regions have relatively high seasonal variability in surface resistances to water mobility, while arid deserts and regions of permanent ice and snow maintain relatively persistent low water mobility, high surface resistance conditions.

Future Sensors

A number of recent and planned satellite sensors potentially satisfy the spatial and temporal demands for global monitoring of terrestrial water mobility. The NASA EOS MODIS sensors onboard Terra and Aqua satellites provide both LST and spectral vegetation index information twice daily on a global basis useful for derivation of surface resistances (Nishida *et al.*, 2003). These data are strongly degraded by the presence of clouds and other atmospheric aerosols as well as low solar illumination, shadowing, and the presence of snow cover that often occur at high latitudes and upper elevations. However, the two MODIS sensors operating in tandem onboard Terra and Aqua offer potential for twice daily global observations at relatively high (1 km) spatial resolution (•Justice *et al.*, 1998). MODIS also has improved spectral and radiometric resolution compared to older NOAA AVHRR series data. Operational continuity of MODIS capabilities will be provided by the NPOESS (National Polar Orbiting Environmental Satellite System) designed for global daily coverage in the 1330 h overpass time, and scheduled for first launch in 2010 (Townshend and Justice, 2002). NPOESS will have a sensor, VIIRS (Visible Infrared Imager/Radiometer Suite) that will have equivalent spectral capabilities of MODIS in visible, infrared, and thermal infrared wavelengths.

Satellite microwave remote sensing also offers the potential for continuous monitoring of the land surface, with direct sensitivity to landscape moisture, freeze–thaw state and aerodynamic roughness for monitoring landscape water mobility. The NOAA SSM/I sensor series has been providing global daily observations since 1988 at coarse (~25 km) spatial scales (Armstrong and Brodzik, 1995). The AMSR-E sensor recently launched onboard the NASA Aqua satellite also provides global daily observations at similar spatial scales (Kawanishi *et al.*, 2003). Active microwave sensors such as SeaWinds, ERS, and Radarsat are also available and offer the potential for global mapping of freeze–thaw state and surface aerodynamic roughness at spatial resolutions on the order of 25 km or less (McDonald *et al.*, 2004; Way *et al.*, 1997; Le Toan *et al.*, 1992).

The National Aeronautics and Space Administration (NASA) is scheduled to launch the Hydrosphere States Mission (HYDROS) in 2010. This combined active–passive microwave remote sensing satellite is specifically designed to study the state of the global terrestrial hydrosphere including soil moisture and freeze–thaw state (Entekhabi *et al.*, 2004). The HYDROS L-band sensors will provide global mapping of landscape freeze–thaw state at spatial and temporal scales of 3 km and 1 to 3 days. Surface (<5 cm) soil moisture will also be distinguished to within 4% volumetric accuracy, allowing discrimination between dry and saturated conditions over the sparsely vegetated areas of the global land surface at spatial and temporal scales of 10 km and 3 days or less. More importantly, the HYDROS sensor will provide an integrated surface resistance measure that will give full global coverage under all conditions of cloud cover, solar illumination, and vegetation cover through integration of optical/thermal and microwave-based algorithms as discussed here.

The sensitivity of these data to different and complementary landscape biophysical variables such as surface temperature, soil moisture, photosynthetic leaf area and vegetation stress provide a potentially effective means for monitoring ecological controls to surface resistance and water mobility for regional hydro-meteorological research and future water management.

Acknowledgments

We acknowledge financial support from NASA Earth Science Enterprise, and contributions to the text from Drs. Ramakrishna Nemani, Hirofumi Hashimoto, and Maosheng Zhao.

FURTHER READING

Carlson T.N., Gillies R.R. and Schmugge T.J. (1995) An interpretation of methodologies for indirect measurement of soil water content. *Agricultural and Forest Meteorology*, **77**, 191–205.

Eagleson P. (2002) *Ecohydrology*, Cambridge University Press: p. 443.

Running S.W., Nemani R.R., Heinsch F.A., Zhao M., Reeves M. and Hashimoto H. (2004) A continuous satellite-derived measure of global terrestrial primary production. *Bioscience*, **54**, 547–560.

Vogelmann J.E., Howard S.M., Yang L., Larson C.R., Wylie B.K. and Van Driel N. (2001) Completion of the 1990s National Land Cover Data Set for the Conterminous United States from Landsat Thematic Mapper Data and Ancillary Data Sources. *Photogrammetric Engineering and Remote Sensing*, **67**, 650–652.

Way J.B., Rignot E., Oren R., Kwok R., McDonald K., Dobson M.C., Bonan G., Viereck L. and Roth J.E. (1994) Evaluating the type and state of Alaskan taiga forests with imaging radar to use in ecosystem flux models. *IEEE Transactions in Geoscience and Remote Sensing*, **32**, 353–370.

REFERENCES

Albertson J.D. and Parlange M.B. (2000) Natural integration of scalar fluxes from complex terrain. *Advances in Water Resources*, **23**(3), 239–252.

Armstrong R.L. and Brodzik M.J. (1995) An earth-gridded SSM/I data set for cryospheric studies and global change monitoring. *Advances in Space Research*, **16**(10), 155–163.

Band L.E., Patterson P., Nemani R.R. and Running S.W. (1993) Forest ecosystem processes at the watershed scale: incorporating hillslope hydrology. *Agriculture Forest Meteorology*, **63**, 93–126.

Bonan G. (2002) *Ecological Climatology*, Cambridge University Press: p. 678.

Bonan G.B., Chapin F.S. and Thompson S.L. (1995) Boreal forest and tundra ecosystems as components of the climate system. *Climatic Change*, **29**, 145–167.

Chapin F.S. III, McGuire A.D., Randerson J., Pielke R. Sr., Baldocchi D., Hobbie S.E., Roulet N., Eugster W., Kasischke E., Rastetter E.B. and Running S.W.(2000) Arctic and boreal ecosystems of western North America as components of the climate system. *Global Change Biology*, **6**,: 211–223.

Diak G.R., Mecikalski J.R., Anderson M.C., Norman J.M., Kustas W.P., Torn R.D. and DeWolf R.L. (2004) Estimating land surface energy budgets from space: Review and current efforts at the University of Wisconsin-Madison and USDA-ARS. *Bulletin of the American Meteorological Society*, **85**, 65–78.

Dickinson R.E. (1996) Land surface processes and climate modeling. *Bulletin of the American Meteorological Society*, **76**, 1445–1448.

El-Rayes M.A. and Ulaby F.T. (1987) Microwave dielectric spectrum of vegetation, Part I: Experimental observations. *IEEE Transactions in Geoscience and Remote Sensing*, **GE-25**(5), 541–549.

Entekhabi D., Njoku E., Houser P., Spencer M., Doiron T., Smith J., Girard R., Belair S., Crow W., Jackson T., *et al.* (2004) The Hydrosphere State (HYDROS) Mission Concept: An earth system pathfinder for global mapping of soil moisture and land freeze/thaw. *IEEE Transactions in Geoscience and Remote Sensing*, **42**, 2181–2195. (in press).

Q15 Friedl M., •*et al.* (2002) Global landcover mapping from MODIS: algorithms and some early results. *Remote Sensing of Environment*, **83**, 287–302.

Gillies R.R., Carlson T.N., Cui J., Kustas W.P. and Humes K.S. (1997) A verification of the 'triangle' method for obtaining surface soil water content and energy fluxes from remote measurements of the Normalized Difference Vegetation Index (NDVI) and surface radiant temperature. *International Journal of Remote Sensing*, **18**(15), 3145–3166.

Goward S.N., Xue Y. and Czajkowski K.P. (2002) Evaluating landsurface moisture conditions from the remotely sensed temperature/vegetation index measurements. *Remote Sensing of Environment*, **79**, 225–242.

Grier C. and Running S.W. (1977) Leaf area of mature northwestern coniferous forests: relation to site water balance. *Ecology*, **58**(4), 893–899.

Hansen M.C., DeFries R.S., Townshend J.R.G., Sohlberg R., Dimiceli C. and Carroll M. (2002) Towards an operational MODIS continuous field of tree cover algorithm: examples using AVHRR and MODIS data. *Remote Sensing of Environment*, **83**, 303–319.

Hashimoto H., Nemani R.R., Yang F. and Running S.W. (2004) Estimation of vapor pressure deficits at the land surface using radiometric temperatures from MODIS. *Remote Sensing of Environment*, (•submitted). Q16

Kane D.L., Hinzman L.D., Haofang Y. and Goering D.J. (1996) The use of SAR satellite imagery to measure active layer moisture contents in arctic Alaska. *Nordic Hydrology*, **27**(1–2), 25–38.

Kawanishi T., Imaoka K., Sezai T., Ito Y.l, Shibata A., Miura M., Inahata H. and Spencer R. (2003) The advanced microwave scanning radiometer for the earth observing system (AMSR-E), NASDA's contribution to the EOS for global energy and water cycle studies. *IEEE Transactions in Geoscience and Remote Sensing*, **41**, 184–194.

Kergoat L. (1998) A model for hydrologic equilibrium of leaf area index on a global scale. *Journal of Hydrology*, **212–213**, 268–286.

Kimball J.S., McDonald K., Keyser A.R., Frolking S. and Running S.W. (2001) Application of the NASA Scatterometer (NSCAT) for determining the daily frozen and nonfrozen landscape of Alaska. *Remote Sensing of Environment*, **75**, 113–126.

Kimball J.S., McDonald K.C., Running S.W. and Frolking S.E. (2004) Satellite radar remote sensing of seasonal growing seasons for boreal and subalpine evergreen forests. *Remote Sensing of Environment*, **90**, 243–258.

Kraszewski A. (1996) *Microwave Aquametry: Electromagnetic Wave Interaction With Water-Containing Materials*, IEEE Press: Piscataway.

Le Toan T., Beaudoin A., Riom J. and Guyon D. (1992) Relating forest biomass to SAR data. *IEEE Transactions in Geoscience and Remote Sensing*, **30**(2), 403–411.

McDonald K.C., Kimball J.S., Njoku E., Zimmermann R. and Zhao M. 2004 Variability in springtime thaw in the terrestrial high latitudes: Monitoring a major control on the biospheric assimilation of atmospheric CO_2 with spaceborne microwave remote sensing. Earth Interactions (•In press). Q17

Moran M.S., Clarke T.R., Inoue Y. and Vidal A. (1994) Estimating crop water deficit using the relation between surface air temperature and spectral vegetation index. *Remote Sensing of Environment*, **49**, 246–263.

Myneni R.B., Hoffman S., Knyazikhin Y., Privette J., Glassy J., Tian Y., Wang Y., Song X., Zhang Y., Smith G.R., etal (2002) Global products of vegetation leaf area and fraction absorbed PAR from year one of MODIS data. *Remote Sensing of Environment*, **83**, 214–231.

Norman J.M., Anderson M.C., Kustas W.P., French A.N., Mecikalski J.R., Torn R., Diak G.R., Schmugge T. and Tanner B.C.W. (2003) Remote sensing of surface energy fluxes at 10-m pixel resolutions. *Water Resources Research*, **39**, 1221, doi:10.1029/2002WR001775.

Nemani R., Keeling C., Hashimoto H., Jolly W., Piper S., Tucker C., Myneni R. and Running S. (2003) Climate-Driven

Increases in Global Terrestrial Net Primary Production from 1982 to 1999. *Science*, **300**, 1560–1563.

Nemani R.R., Pierce L.L. and Running S.W. (1993) Developing satellite-derived estimates of surface moisture status. *Journal of Applied Meteorology*, **32**, 548–557.

Q18 Nemani R.R. and Running S.W. (•1989a) Estimation of regional surface resistance to evapotranspiration from NDVI and thermal infrared AVHRR data. *Journal of Applied Meteorology*, **28**, 276–284.

Nemani R.R. and Running S.W. (1989b) Testing a theoretical climate-soil-leaf area hydrologic equilibrium of forests using satellite data and ecosystem simulation. *Agriculture and Forest Meteorology*, **44**, 245–260.

Nemani R.R. and Running. S.W. (1997) Land cover characterization using multi-temporal red, near-IR and thermal-IR data from NOAA/AVHRR. *Ecological Applications*, **7**, 79–90,1560–1563.

Nielson R.P. (1995) A model for predicting continental-scale vegetation distribution and water balance. *Ecological Applications*, **5**, 362–385.

Nishida K., Nemani R.R., Glassy J.M. and Running S.W.

Q19 (•2003a) Development of an evapotranspiration index from Aqua/MODIS for monitoring surface moisture status. *IEEE Transactions on Geoscience and Remote Sensing*, **41**(2), 493–501.

Nishida K., Nemani R., Running S. and Glassy J. (2003b) An Operational Remote Sensing Algorithm of Land Surface Evaporation. *Journal of Geophysical Research*, **108**(D9), 4270,10.1029/2002JD002062.

Pitman A.J. (2003) The evolution of, and revolution in, land surface schemes designed for climate models. *International Journal of Climatology*, **23**, 479–510.

Prentice I.C., Cramer W., Harrison S.P., Leemans R., Monserud R.A. and Solomon A.M. (1992) A global biome model based on plant physiology and dominance, soil properties and climate. *Journal of Biogeography*, **19**, 117–134.

Running S.W. and Coughlan J.C. (1988) A general model of forest ecosystem processes for regional applications. *Ecological Modeling*, **42**, 125–154.

Sandholt I., Rasmussen K. and Anderson J. (2002) A simple interpretation of the surface temperature/vegetation index space for assessment of surface moisture status. *Remote Sensing of Environment*, **79**, 213–224.

Schmugge T.J., Kustas W.P., Ritchie J.C., Jackson T.J. and Rango A. (2002) Remote sensing in hydrology. *Advances in Water Resources*, **25**, 1367–1385.

Sellers P.J., Mintz Y., Sud Y.C. and Dalcher A. (1986) A simple biosphere model for use with general circulation models. *Journal of the Atmospheric Sciences*, **43**, 505–531.

Stephenson N.L. (1990) Climatic control of vegetation distribution: The role of the water balance. *The American Naturalist*, **135**(5), 649–670.

Townshend J.R.G. and Justice C.O. (2002) Towards operational monitoring of terrestrial systems by moderate resolution remote sensing. *Remote Sensing of Environment*, **83**, 351–359.

Ulaby F.T., Moore R.K. and Fung A.K. (1986) *Microwave Remote Sensing-Active and Passive*, Vol. III, Artec House: Dedham.

Vorosmarty C.J., Federer C.A. and Schloss A.L. (1998) Potential evaporation functions compared on U.S. watersheds. Possible implications for global-scale water balance and terrestrial ecosystem modeling. *Journal of Hydrology*, **207**, 147–169.

Walter H. (1979) *Vegetation of the Earth and Ecological Systems of the Geo-Biosphere*, *Second Edition*, Springer-Verlag: New York.

Wan Z.M., Zhang Y., Zhang Q. and Li Z. (2002) Validation of the land surface temperature retrieved from Terra MODIS data. *Remote Sensing of Environment*, **83**, 163–180.

Waring R. and Running S.W. (1998) *Forest Ecosystems: Analysis at Multiple Scales*, Academic Press: San Diego.

Waring R.H., way J.B., Hunt E.R., Morrissey L., Ranson K.J., Weishampel J.F., Oren R. and Franklin S.E. (1995) Imaging radar for ecosystem studies. *Bioscience*, **45**(10), 715–723.

Way J.B., Zimmermann R., Rignot E., McDonald K. and Oren R. (1997) Winter and spring thaw as observed with imaging radar at BOREAS. *Journal of Geophysical Research*, **102**, 29,673–29,684.

Woodward F.I. (1987) *Climate and Plant Distribution*, Cambridge Univ Press: p. 174.

Zhang T., Scambos T., Haran T., Hinzman L.D., Barry R.G. and Kane D.L. (2003) Ground-based and satellite derived measurements of surface albedo on the north slope of Alaska. *Journal of Hydrometeorology*, **4**, 77–91.

Keywords: evapotranspiration; surface resistance; drought; freeze–thaw; remote sensing; vegetation; MODIS; HYDROS